A Compact Transmission-Line Metamaterial Antenna With Extended Bandwidth

Jiang Zhu, *Student Member, IEEE*, and George V. Eleftheriades, *Fellow, IEEE*

***Abstract*—A wideband and compact planar antenna is proposed using a doubly resonant transmission-line metamaterial (TL-MTM) structure. The antenna consists of two TL-MTM arms that resonate at different frequencies. Each arm comprises a microstrip transmission-line loaded with five spiral inductors and is well matched to 50 Ω through an embedded series meandered line. Each arm is designed to work as a single antenna at its own resonant frequency, determined by the loading spiral inductance, where a zero insertion phase occurs. A wideband antenna matching is enabled when these two resonances suitably merge together. A fabricated prototype has dimensions of $\lambda_o/4 \times \lambda_o/7 \times \lambda_o/29$, yielding a vertical linear electric field polarization, and provides a 100-MHz bandwidth (−10 dB) with a measured radiation efficiency of 65.8% at 3.30 GHz.**

***Index Terms*—Compact antennas, meandered line inductor, metamaterials, spiral inductor.**

I. Introduction

COMPACT antennas are important for today's mobile communication systems. The typical difficulties encountered when designing compact antennas include narrow bandwidth, impedance matching to a low radiation resistance, and low radiation efficiency [1]. Transmission-line metamaterials (TL-MTM) [2] provide a conceptual route for implementing small resonant antennas [3]–[9]. The first proposals of using TL-MTM structures at resonance to implement small printed antennas have been documented in [4] and [5]. However, TL-MTM antennas typically suffer from narrow bandwidths [3]–[9]. This letter addresses the bandwidth problem by proposing a two-arm TL-MTM antenna, resonating at two closely spaced frequencies.

The proposed antenna is based on a microstrip transmission-line that is periodically loaded with shunt spiral inductors, leading to a fully printed resonant metamaterial antenna operating around 3 GHz. The corresponding resonance occurs at the point of 0° phase shift between cells, where the resonant frequency is independent of the number of the unit cells [4]–[9]. A series meandered-line inductor is employed to compensate the capacitive input impedance in order to achieve a good impedance matching to 50 Ω, while an additional match network is not needed. As shown in Fig. 1, the proposed antenna consists of two TL-MTM arms. Each arm can work independently at its own operating frequency. A wideband performance is achieved by merging the corresponding two resonances together in a single passband. This can be realized by a small perturbation in the number of turns of one arm's spiral inductors. The experimental results show that the bandwidth is more than doubled, compared to the single arm operation. Moreover, a vertically polarized radiation pattern is observed and a reasonable radiation efficiency is obtained.

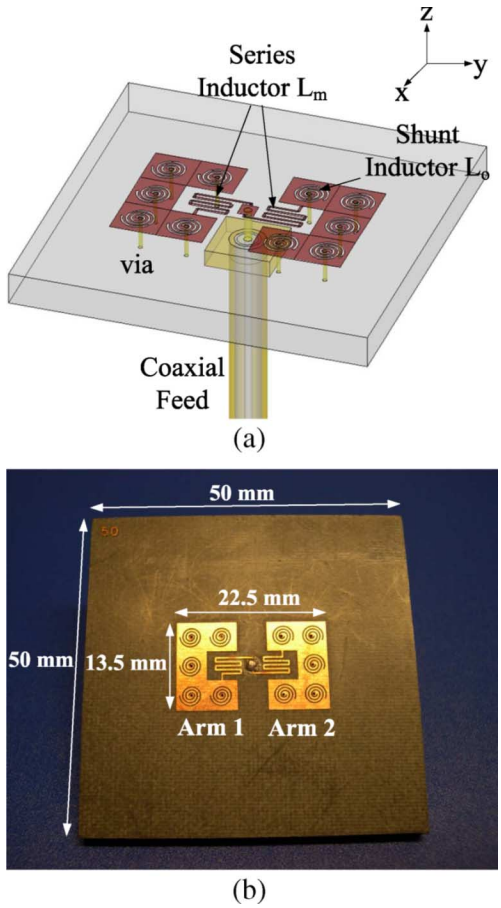

Fig. 1. The proposed two-arm TL-MTM antenna featuring a compact size and extended bandwidth: (a) 3D schematic and (b) top-view photograph of the fabricated prototype.

II. Proposed Design

A. Proposed TL-MTM Unit Cell

The antenna is implemented using a microstrip line, which is printed on a Rogers RT/duriod 5880 ($\varepsilon_r = 2.2$, $\tan\delta = 0.0009$) substrate with a thickness of 3.175 mm (125 mil). The

Manuscript received October 23, 2008; revised November 26, 2008. First published December 09, 2008; current version published May 13, 2009. This work was supported by the Natural Sciences and Engineering Research Council of Canada (NSERC).

The authors are with the Edward S. Rogers Sr. Department of Electrical and Computer Engineering, University of Toronto, Toronto, ON M5S 3G4, Canada (e-mail: jiangzhu@waves.utoronto.ca; gelefth@waves.utoronto.ca).

Color versions of one or more of the figures in this letter are available online at http://ieeexplore.ieee.org

Digital Object Identifier 10.1109/LAWP.2008.2010722

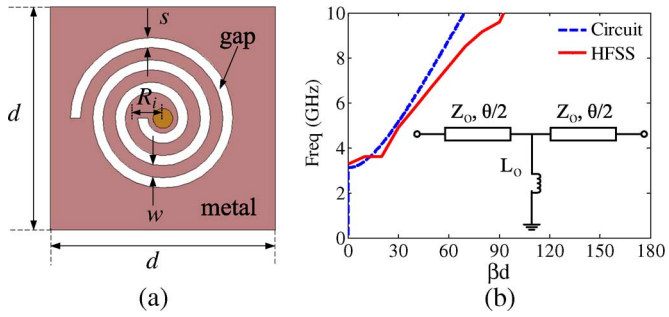

Fig. 2. Proposed spiral-inductor-loaded TL-MTM unit cell. (a) Geometry of the unit cell; (b) transmission-line representation.

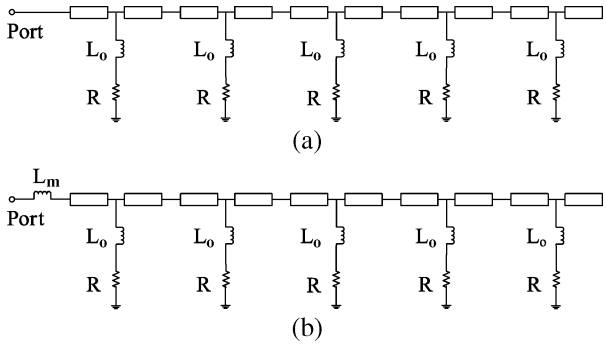

Fig. 3. Circuit models for the proposed one-arm TL-MTM antenna. (a) Circuit model for one-arm metamaterial compact antenna without matching. (b) Circuit model for one-arm metamaterial compact antenna with matching.

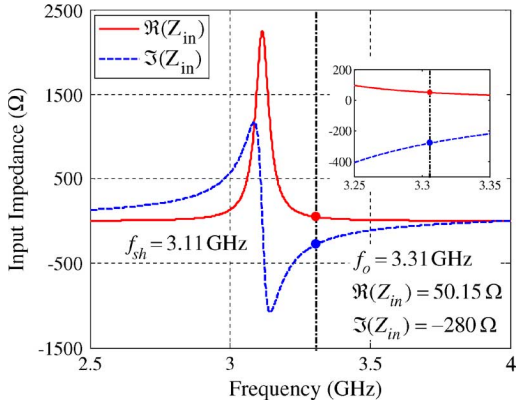

Fig. 4. Input impedance response of the one-arm TL-MTM antenna obtained from the circuit analysis of the model shown in Fig. 3(a).

unit cell shown in Fig. 2 has dimensions of $d \times d = 4.5 \times 4.5$ mm^2. The corresponding host transmission line characteristic impedance and electrical length per cell are denoted as Z_o and θ, respectively. The printed unit-cell element employs round spiral inductors as shown in Fig. 2(a). The feature sizes of the spiral inductor—including the conductor width w, the conductor spacing s, the inner radius (to the center of the conductor) $R_{\rm i}$, and the number of turns N—determine the inductance. A smaller feature size results in a larger inductance, and, at the same time, a larger conductor loss, which affects the antenna's radiation efficiency performance. The spiral inductor is connected to the ground through a via that has a radius of 0.2 mm. The overall shunt inductance $L_{\rm o}$ is the combination of the spiral and shorting via inductances, although the latter contributes a small amount compared to the spiral inductance. The proposed design keeps the overall size of the unit cell compact while aiming to reduce the Ohmic loss (to improve radiation efficiency). The design parameters are $w = 0.25$ mm, $s = 0.2$ mm, $R_{\rm i} = 0.6$ mm, and $N = 2$. The corresponding dispersion diagram can be found using periodic circuit analysis, as shown in Fig. 2(b). In the circuit model, the embedded microstrip spiral inductor is modeled as a single shunt inductor for simplicity, while the parasitic effects are ignored, which results in the discrepancies between the full-wave Ansoft's HFSS model and the circuit model in the dispersion diagram. The corresponding TL-MTM can be considered a negative permittivity medium [2], with the corresponding plasma frequency given by

$$f_{\rm sh} = \frac{1}{2\pi\sqrt{L_{\rm o}C}}. \tag{1}$$

Here, C is the intrinsic capacitance per unit length of the host TL. For a specified unit cell, (1) can be used to determine the loading shunt inductance value of $L_{\rm o}$ required to produce a shunt resonant frequency at $f_{\rm sh}$.

B. One-Arm Antenna Design

The proposed one-arm antenna consists of five cascaded spiral-inductor-loaded unit cells. It can be analyzed by its equivalent circuit model shown in Fig. 3(a). The resistance R represents the antenna resistance that contains two parts: the radiation resistance $R_{\rm r}$ and the loss resistance $R_{\rm l}$. The circuit response is a function of the design parameters $L_{\rm o}$ and R. By matching this circuit response to the response from HFSS through optimization, the extracted circuit parameters are $L_o = 10.25$ nH and $R = 2\ \Omega$, respectively. A typical impedance response with real and imaginary parts is given in Fig. 4. At the resonant frequency $f_{\rm sh}$, where the real part of the input impedance reaches its maximum value, the real and imaginary parts of the input impedance are large and sensitive to frequency variations, which makes the impedance matching at this frequency practically difficult.

One can observe that at frequencies higher than the resonant frequency $f_{\rm sh}$, $\Re(Z_{\rm in})$ decreases dramatically. At a certain frequency $f_{\rm o}$, $\Re(Z_{\rm in}) = 50\ \Omega$, while $\Im(Z_{\rm in})$ is capacitive. Therefore, a series inductance L_m can be used to match the antenna to 50 Ω. The required series inductance of L_m is given by

$$L_m = \frac{\Im\left(Z_{\rm in}(f_{\rm o})\right)}{2\pi f_{\rm o}}. \tag{2}$$

As demonstrated in Fig. 4, at the operating frequency $f_{\rm o} = 3.31$ GHz, $\Im(Z_{\rm in}) = -280\ \Omega$, which leads to the series inductance $L_m = 13.5$ nH, according to (2). In practice, the matching series inductor can be implemented by a meandered-line inductor. The operating frequency $f_{\rm o}$ is very close to the resonant frequency $f_{\rm sh}$, which ensures similar field distributions at these two frequencies. Besides, unlike [8], the matching network is directly applied when $\Re(Z_{\rm in}) = 50\ \Omega$, and therefore an impedance transformer is not necessary. Finally, since the proposed antenna operates at the frequencies where the input impedance remains flat, compared to operating at $f_{\rm sh}$, the obtained bandwidth is expected to be improved.

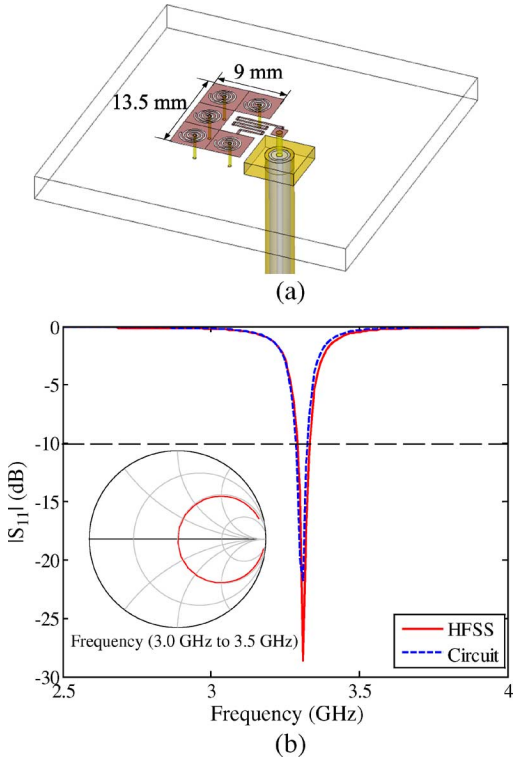

Fig. 5. (a) Proposed one-arm resonant TL-MTM antenna layout, and (b) the simulated return loss from Ansoft's HFSS analysis and from the circuit analysis of the model shown in Fig. 3(b).

The geometry of the proposed one-arm antenna is shown in Fig. 5(a). It consists of five spiral-inductor-loaded unit cells and one series meandered-line inductor. The width of the meandered line is 0.25 mm, and its length is adjusted in order to compensate the capacitive imaginary part of the input impedance and create a good match to 50 Ω. The unit cells are connected with right-angle bends to obtain a compact topology without changing the characteristics of the performance. The end of the meandered line is connected to a coaxial feed, whereas the size of the one-arm antenna is 13.5 mm × 9.0 mm, corresponding to $\lambda_o/7 \times \lambda_o/11$ in electrical length. As indicated in Fig. 2(b), the phase shift per unit cell at f_o is 3°. The simulated return loss from Ansoft's HFSS is given in Fig. 5(b), which shows that the proposed one-arm antenna has a good impedance match at the frequency of 3.31 GHz, and the corresponding −10-dB bandwidth is about 40 MHz.

C. Two-Arm Antenna Design

The proposed two-arm antenna is shown in Fig. 1. The two arms are axially symmetric to the coaxial feed at the center of the antenna and are identical except that the number of turns of the spiral inductors has a $\Delta N = |N_1 - N_2|$ turn difference, which results in a difference in the loading shunt inductance of ΔL_o. As seen from the previous section, each arm operates independently and the operating frequency f_o is determined by the loading inductance of the spiral-inductor. Therefore, the proposed two-arm antenna is well suited for dual resonance applications. For a small turn detuning ΔN, the frequency shift of the operating frequencies for the two arms $\Delta f_o = |f_{o1} - f_{o2}|$ is small enough such that the two resonances merge together in a single passband, which enables the broadband operation of the resonant TL-MTM antenna. Furthermore, the two arms are set 4.5 mm (one unit-cell size) apart in order to reduce the mutual coupling between the two arms.

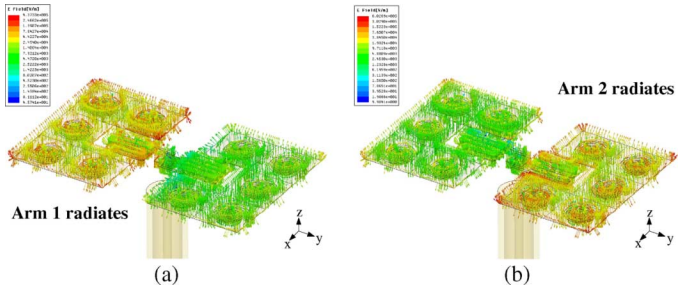

Fig. 6. E-field distribution of the proposed two-arm resonant metamaterial antenna obtained from Ansoft's HFSS: (a) Arm 1 radiates when the antenna operates at $f_{o1} = 3.25$ GHz; (b) Arm 2 radiates when the antenna operates at $f_{o2} = 3.31$ GHz.

As shown in Fig. 1, the metallic area of the two-arm antenna is 22.5×13.5 mm^2. For a size of a ground plane smaller than 40×40 mm^2, parasitic currents begin to flow on the outer conductor of the coaxial cable. Thus, a conservative 50×50 mm^2 ground plane is used to avoid the need for an external balun [7]. Fig. 6 shows the electric field distributions along the metallic surfaces obtained from Ansoft's HFSS when $\Delta N = 0.07$. It can be seen that the two arms have a good isolation, and each arm is activated only at its corresponding operating frequency.

Since each arm of the antenna resonates at a different frequency, the proposed two-arm topology is also suitable for dual-band applications simply by tuning the number of the turns N_1 and N_2, respectively, in order to obtain proper loading inductances according to (2). In this case, the matching series inductance L_m has to be adjusted separately in order to achieve the impedance matching for each arm.

III. Simulation and Measurement Results

The measured versus the simulated return loss from HFSS for the two-arm antenna is shown in Fig. 7. It can be seen that the antenna is well matched from 3.23 to 3.33 GHz, which results in a measured return loss bandwidth (−10 dB) of 100 MHz. This corresponds to approximately 3.1%, which is more than double that of the constituent single-arm antenna. A suitably merged double resonance in the frequency range of 3.25 to 3.30 GHz can be clearly observed within the passband.

For comparison, a coaxially fed patch antenna is designed at the same resonant frequency and on the same substrate. As shown in Table I, the proposed two-arm TL-MTM antenna has a comparable fractional bandwidth (FBW) with that of a single patch antenna. However, the area of the proposed MTM patch exhibits a significant size reduction compared to the conventional patch size.

Fig. 8 shows the simulated and measured E-plane and H-plane radiation patterns at the higher operating frequency of 3.30 GHz; similar radiation patterns are obtained at the lower operating frequency of 3.25 GHz when Arm 1 radiates. The proposed antenna exhibits a radiation pattern with a vertical linear electric field polarization similar to that of a short monopole (or

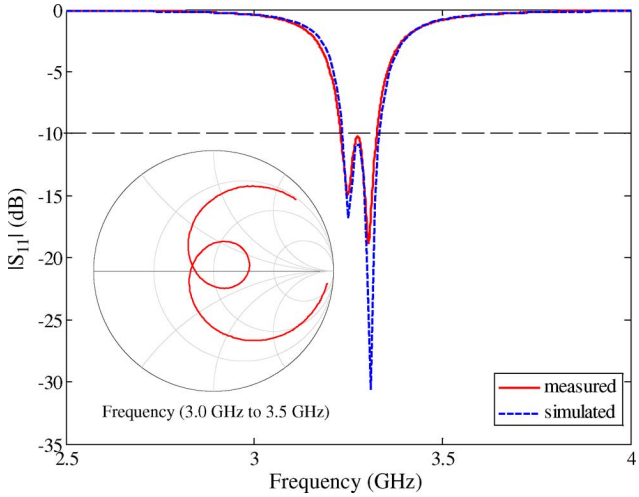

Fig. 7. Measured and HFSS simulated return loss for the proposed two-arm antenna. A double resonance pattern is clearly observed within the passband.

TABLE I
COMPARISON OF SIZE AND BANDWIDTH FOR PATCH ANTENNA, TWO-ARM TL-MTM ANTENNA, AND SINGLE-ARM TL-MTM ANTENNA WITH THE SAME RESONANT FREQUENCY

	Physical Size	Metallic Area	Area Saving	FBW
Patch	28.5×28.5 mm^2	812 mm^2	-	3.7 %
Two-Arm	22.5×13.5 mm^2	304 mm^2	63 %	3.1 %
Single-Arm	13.5×9.0 mm^2	122 mm^2	85 %	1.2 %

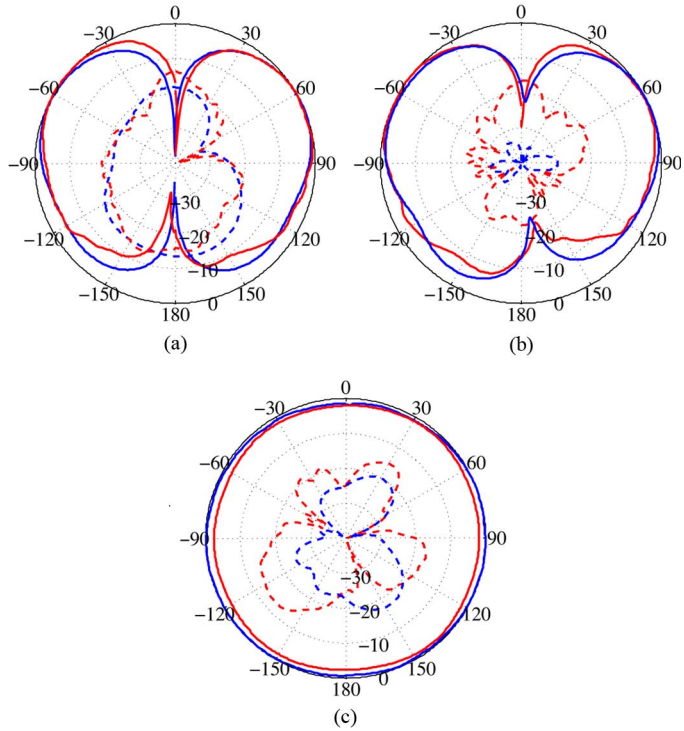

Fig. 8. Normalized radiation patterns for the proposed two-arm antenna at 3.30 GHz: (a) E-plane (*xz*-plane), (b) E-plane (*yz*-plane), and (c) H-plane (*xy*-plane). Light line: measurement; dark line: simulation; solid line: copolarization; dashed line: cross-polarization.

magnetic loop) on a small ground plane [6], [7]. Using the two measured principal E-plane cuts in the *xz*-plane and *yz*-plane, the estimated measured directivity is 1.82 (2.61 dBi), and the measured peak gain using the gain comparison method is 1.20 (0.79 dBi), resulting in a measured efficiency of 65.8%.

IV. CONCLUSION

A wideband and compact resonant transmission-line metamaterial (TL-MTM) antenna is proposed based on the principle of double resonance. The antenna comprises two TL-MTM arms, each consisting of five spiral-inductor-loaded transmission-lines in microstrip. Each arm is designed to work at its own operating frequency, which is adjusted by the loading spiral inductors. A wideband characteristic is enabled when the corresponding two resonant frequencies suitably merge together into one single passband. The theoretical performance is verified by full-wave simulations and experimental data. The fabricated prototype of size $\lambda_o/4 \times \lambda_o/7 \times \lambda_o/29$ exhibits a vertical linear electric field polarization with a reasonable measured efficiency of 65.8% at 3.30 GHz and provides a 100-MHz (-10 dB) bandwidth. By further detuning the two resonant frequencies, the proposed antenna can also be designed for dual-band applications. These attributes make the proposed antenna well suited for emerging wireless applications.

ACKNOWLEDGMENT

The authors would like to thank M. A. Antoniades of the Electromagnetics Group at the University of Toronto for stimulating discussions and T. V. C. T. Chan for assisting in the fabrication and testing of the prototype antenna.

REFERENCES

[1] S. R. Best, "The radiation properties of electrically small folded spherical helix antennas," *IEEE Trans. Antennas Propag.*, vol. 52, no. 4, pp. 953–960, Apr. 2004.
[2] G. V. Eleftheriades, A. K. Iyer, and P. C. Kremer, "Planar negative refractive index media using periodically loaded transmission lines," *IEEE Trans. Microw. Theory Techn.*, vol. 50, no. 12, pp. 2702–2712, Dec. 2002.
[3] G. V. Eleftheriades, "Enabling RF/microwave devices using negative-refractive-index transmission-line (NRI-TL) metamaterials," *IEEE Antennas Propag. Mag.*, vol. 49, no. 2, pp. 34–51, Apr. 2007.
[4] G. V. Eleftheriades, A. Grbic, and M. Antoniades, "Negative-refractive-index transmission-line metamaterials and enabling electromagnetic applications," in *Proc. IEEE Antennas Propag. Soc. Int. Symp. Dig.*, Jun. 2004, pp. 1399–1402.
[5] A. Sanada, M. Kimura, H. Kubo, C. Caloz, and T. Itoh, "A planar zeroth order resonator antenna using a left-handed transmission line," in *Proc. 34th Eur. Microw. Conf. (EuMC)*, Amsterdam, The Netherlands, Oct. 2004, pp. 1341–1344.
[6] F. Qureshi, M. A. Antoniades, and G. V. Eleftheriades, "A compact and low-profile metamaterial ring antenna with vertical polarization," *IEEE Antennas Wireless Propag. Lett.*, vol. 4, pp. 333–336, 2005.
[7] M. A. Antoniades and G. V. Eleftheriades, "A folded-monopole model for electrically small NRI-TL metamaterial antennas," *IEEE Antennas Wireless Propag. Lett.*, vol. 7, pp. 425–428, 2008.
[8] A. Lai, K. Leong, and T. Itoh, "Infinite wavelength resonant antennas with monopolar radiation pattern based on periodic structures," *IEEE Trans. Antennas Propag.*, vol. 55, no. 3, pp. 868–876, Mar. 2007.
[9] J.-G. Lee and J.-H. Lee, "Zeroth order resonance loop antenna," *IEEE Trans. Antennas Propag.*, vol. 55, no. 3, pp. 994–997, Mar. 2007.